Available online at www.sciencedirect.com
ScienceDirect
Intermetallics 15 (2007) 26–33
Intermetallics
www.elsevier.com/locate/intermet

High strength nanocrystalline $L1_2$-Al_3(Ti,Zr) intermetallic synthesized by mechanical alloying

S.S. Nayak [a,*], S.K. Pabi [a], B.S. Murty [b]

[a] Department of Metallurgical and Materials Engineering, Indian Institute of Technology, Kharagpur, West Bengal 721302, India
[b] Department of Metallurgical and Materials Engineering, Indian Institute of Technology, Madras, Chennai 600036, India

Received 10 January 2006; received in revised form 13 February 2006; accepted 14 February 2006
Available online 30 May 2006

Abstract

Nanocrystalline $L1_2$-Al_3(Ti,Zr) intermetallic has been synthesized directly by mechanical alloying of elemental blends of the nominal composition $Al_{75}(Ti_{25-x}Zr_x)$ for $x = 0$, 5, 10, 15, 20 and 25. The long range order parameter is found to increase with the Zr content. The lattice parameter difference between the $L1_2$-Al_3(Ti,Zr) and Al was minimum for the alloy with 10% Zr. A very high hardness of 3.23 GPa was achieved for the $L1_2$ phase in the $Al_{75}Ti_{15}Zr_{10}$ composition in the green compact condition with a relative density of 77.6%.

Keywords: A. Intermetallics, miscellaneous; C. Mechanical alloying and milling; A. Aluminides, miscellaneous

1. Introduction

Ever since its invention, mechanical alloying (MA) has attracted a lot of attention of the materials scientists for the easy synthesis of stable and metastable structures including super saturated solid solution, amorphous phases, quasicrystalline phase, ordered intermetallics and nanocrystalline materials in almost all the alloy systems [1,2] at ambient temperature. MA synthesizes materials with novel properties and homogeneous microstructure starting from elemental blends. Many researchers have reported on the synthesis and stability of intermetallics like aluminides [3,4], silicides [5], nitrides [1], etc., using the MA route. Among all the intermetallics, aluminides are quite popular because of their superior oxidation and corrosion resistance coupled with very high strength to weight ratio and significant research has been reported over the last decade on the synthesis of these aluminides by MA [2].

Al_3Ti, a very popular intermetallic, is used vastly in the structural applications mainly in aerospace industries. However, its room temperature brittleness, due to tetragonal DO_{22} structure, hampers its formability. There is a possibility of improving the ductility if the DO_{22} structure can be transformed into a more symmetric cubic $L1_2$ structure [6]. A number of attempts have been made to stabilize the $L1_2$-Al_3Ti by the addition of ternary elements [6,7]. However, no evidence of superlattice peaks was observed for $L1_2$-Al_3Ti even after heat treatment in the mechanically alloyed samples [7,8]. This has been attributed to the lower diffraction intensity of the superlattice peaks due to the lower difference in the scattering factor of Al and Ti [7–9]. Jang et al. [10] have recently studied the effect of Mn addition on formation of the $L1_2$ phase of Al_3Ti in the composition range of (Al–x at.% Mn)$_3$Ti ($x = 1$–12) by MA and showed that stable $L1_2$ phase is obtained at 8% Mn.

Synthesis of $L1_2$-Al_3Zr by MA has also been reported by a number of investigators [11–15]. Desch et al. [12] have successfully prepared $L1_2$ phase of Al_3Zr using hexane as a process controlling agent during MA. They have used elemental mixture of Al with Zr or ZrH_2 as starting materials for ball milling. In both the cases they found the $L1_2$ phase, the rate of alloying was faster in Al and Zr mixture compared to Al and ZrH_2 mixture. Suryanarayana et al. [13] have reported

* Corresponding author. Tel.: +91 44 22574754.
E-mail addresses: sashank_n@yahoo.com (S.S. Nayak), murty@iitm.ac.in (B.S. Murty).

0966-9795/$ - see front matter © 2006 Elsevier Ltd. All rights reserved.
doi:10.1016/j.intermet.2006.02.003

the synthesis of $L1_2$ phase in $(Al,M)_3Zr$ for M = Fe, Ni by MA. Moon et al. [14] have studied the effect of ternary elements (Cu, Ni, and Mn) on formation and thermal stability of nanocrystalline $L1_2$-Al_3Zr alloy by MA. They found that the addition of Mn leads to the formation of $L1_2$-Al_3Zr after 3 h of MA, which transforms into amorphous after 6 h of MA. Also $L1_2$-Al_3Zr thus formed by the ternary addition was found stable up to 900 °C. Lee et al. [15] have investigated the formation and mechanical properties of the $L1_2$ type bulk (Al−12.5 at.% $M)_3Zr$ (M = Cu, Mn) intermetallics with a nanocrystalline structure by MA.

Apart from MA, other processing techniques, e.g. inert gas condensation (IGC), rapid solidification processing (RSP) and conventional casting, also have been used successfully for the synthesis of metastable $L1_2$ phase and respective equilibrium phases in both Al_3Ti and Al_3Zr either as single phase or as dispersoids in Al matrix [16–20]. Han et al. [17] have reported the effect of Mn addition and Ti:Zr ratio on $Al_{66}Mn_9(Ti,Zr)_{25}$ intermetallics by conventional casting route. The tetragonal $Al_3(Ti_{1-x}Zr_x)$ phase was reported to be transformed by the addition of 9% Mn to the cubic Ll_2-$A1_{66}Mn_9(Ti_{1-x}Zr_x)_{25}$ with a small amount of second phases such as Al_8Mn_5 and Al_2Zr still existing in the as-cast condition. The combined addition of Ti and Zr was found to reduce the hardness of intermetallic alloys compared to the addition of Ti or Zr alone. The Microhardness data are well below those of two $Al_6Mn_9Ti_{25}$ and $Al_6Mn_9Zr_{25}$ compounds. The influence of Zr on structure and properties of Al_3Ti prepared by arc melting has been reported by Karpets et al. [18]. It was reported that with an increase in the concentration of Zr the $D0_{22}$ structure typical to Al_3Ti transforms into the $D0_{23}$ structure. Alloying of the Al_3Ti with Zr and Al_3Zr with Ti decreases hardness and increases plasticity.

Though the work on the synthesis and stability of $L1_2$-Al_3Ti and Al_3Zr have been reported by many researchers, so far there are no such reports on synthesis and characterization of $L1_2$-$Al_3(Ti,Zr)$ compound by MA. In addition, there are no reports on the influence of Zr on ordering behavior of $L1_2$-$Al_3(Ti,Zr)$. The present paper attempts to fill these gaps.

2. Experimental details

Elemental powder blends with nominal compositions of $Al_{75}(Ti_{25-x}Zr_x)$, $x = 0$, 5, 10, 15, 20 and 25 were mechanically alloyed for 20 h in an FRITSCH Pulverisette-5 planetary mill. Al and Zr powders of particle size of less than 45 μm and Ti sponge were used as starting materials. The purity was 99.7% for Al, 99.9% for Zr and 99.5% for Ti. MA was carried out at 300 rpm in tungsten carbide (WC) container in toluene using 10 mm diameter WC balls keeping the ball to powder weight ratio as 10:1. After regular intervals of MA, powders were taken out for characterizations. Phase analysis of the mechanically alloyed samples was done by X-ray diffraction (XRD) using Co-K_α radiation in a PHILIPS 1729 X-ray diffractometer. The effective crystallite size of mechanically alloyed powders was determined using the Voigt single line method [21] after eliminating the contribution of instrumental broadening. The nanocrystalline nature and the ordered structure were confirmed by transmission electron microscopic (TEM) analysis using PHILIPS CM20 electron microscope. The long range order parameter (S) was calculated considering the (110) superlattice reflection and (111) fundamental reflection of cubic $L1_2$ structure formed by MA using the following formula:

$$S = \sqrt{\frac{\left(I_{(110)}/I_{(111)}\right)_{\text{obs}}}{\left(I_{(110)}/I_{(111)}\right)_{\text{std}}}}$$

where subscripts ''obs'' and ''std'' stand for Observed and Standard ratios of the intensities of the mentioned diffracting atomic planes. Here standard ratio refers to that for a completely ordered structure. The powder diffraction data for $L1_2$ structure of both Al_3Ti and Al_3Zr are not available in the standard JCPDS file and hence the relative intensity of the superlattice reflections for the completely ordered structure (standard ratio) is not known. Hence, it is difficult to find out long rang order parameter of $L1_2$ Al_3Ti and Al_3Zr prepared in

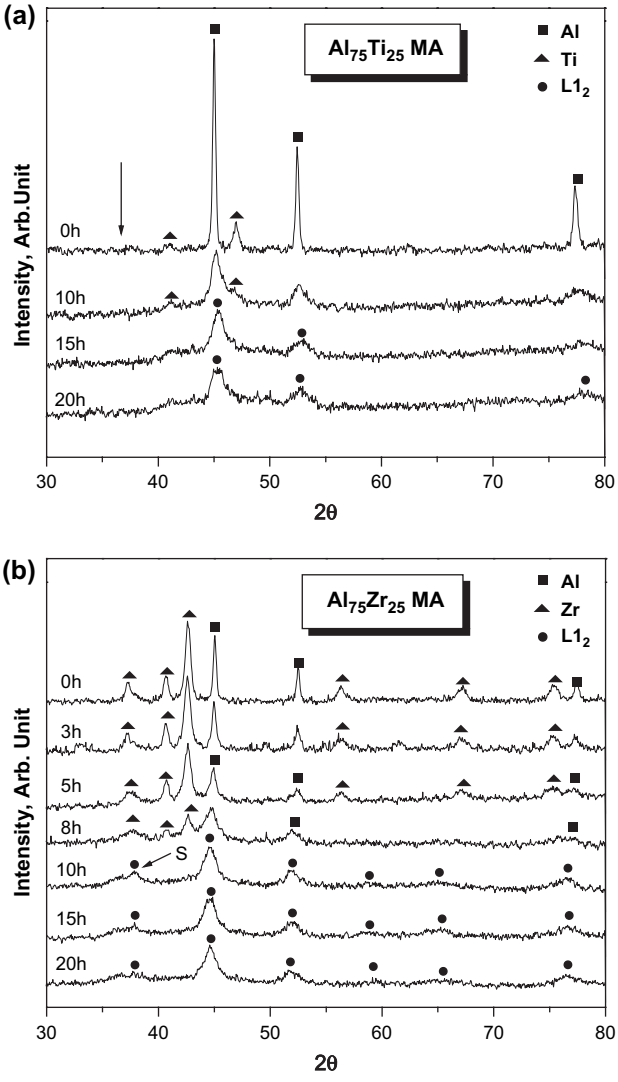

Fig. 1. XRD patterns of (a) $Al_{75}Ti_{25}$ and (b) $Al_{75}Zr_{25}$ after different durations of MA.

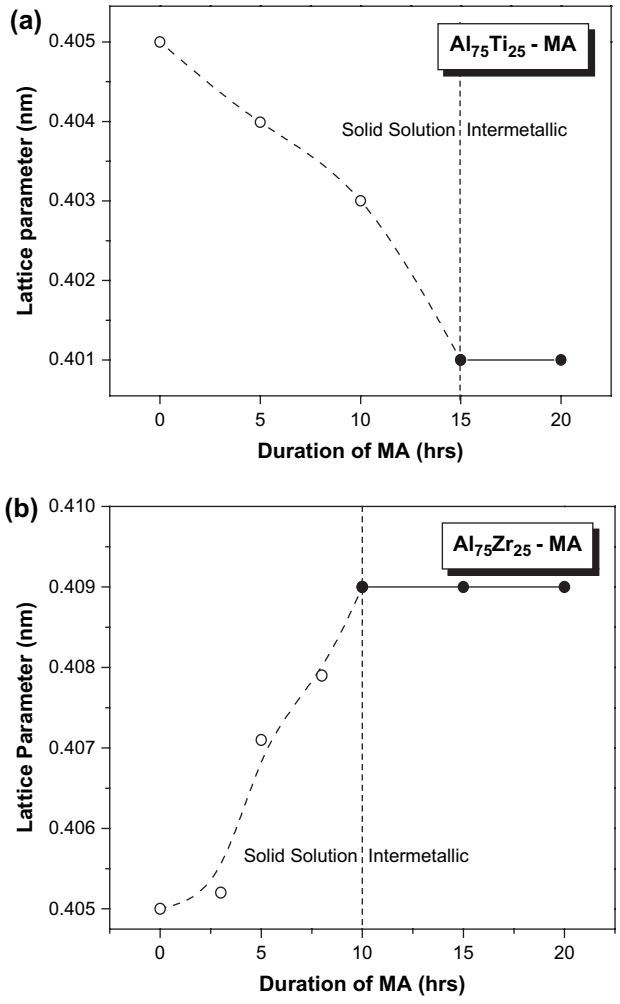

Fig. 2. Variation of lattice parameter of (a) $Al_{75}Ti_{25}$ and (b) $Al_{75}Zr_{25}$ as function of duration of MA.

the present study directly from XRD diffractograms, using the above-mentioned formula. Hence, the relative intensity ratio of superlattice and fundamental reflections was calculated theoretically using atomic scattering factors of all the elements with the help of the simple formula given by Culity [22]:

$$\frac{\text{Intensity(superlattice)}}{\text{Intensity(fundamental)}} \approx \frac{|F_s|^2}{|F_f|^2} = \frac{(f_{\text{TM}} - f_{\text{Al}})^2}{(f_{\text{TM}} + 3f_{\text{Al}})^2}$$

where F is the structure factor and f is the atomic scattering factor, which has been assumed equivalent to the atomic number. In the above equation, the subscript TM stands for the transition metal Ti or Zr. Calculations based on the above formula show that the intensities of (110) superlattice peak of fully ordered $L1_2$-Al_3Zr and $L1_2$-Al_3Ti intermetallics are 12% and 2%, respectively, of that of the intensity of the (111) fundamental reflection. A linear relationship between the intensity ratios and Zr content in the nominal composition was assumed and these values were used for calculating the LRO of the ternary compositions.

The MA powders were consolidated into cylindrical shapes of 12 mm diameter using 375 MPa (5.5 t) of load with a loading time of 15 s. The density of the pellets was measured using the Archimedes' principle. The micro Vickers hardness was measured under a load of 300 g with dwelling time of 15 s using a LECO DM-400 hardness tester.

3. Results and discussion

The XRD patterns for binary nominal composition $Al_{75}Ti_{25}$ after different durations of MA are shown in Fig. 1(a). Unmilled powder (0 h) sample shows the elemental peaks of both Al and Ti. Ti peaks appear after 10 h of MA though their relative intensity reduced suggesting the formation of Al(Ti) solid solution. In general, 1 at.% Ti decreases the lattice parameter of Al (0.405 nm) by 0.001 nm [23]. After 10 h of MA, the lattice parameter of Al (0.403 nm) suggests that 2 at.% Ti was dissolved in Al, which is quite higher than the room temperature solubility of Ti in Al. After 15 h of MA all the elemental peaks disappear and a new phase with broad peak at 2θ of 45.3° was observed. A shift in the peaks of Al towards the higher diffraction angle has been observed with increase in the duration of MA indicating a continuous decrease in the lattice parameter of Al. The lattice parameter after 15 h of MA matches exactly with the previously reported value for binary $L1_2$-Al_3Ti [7–9]. The $L1_2$ phase thus formed was found to be stable on further milling up to 20 h. Besides their shift, the peaks were broadened with the duration of MA, which can be attributed to the refinement of the crystallites. The crystallite size was found to decrease significantly at the early hours of MA and becomes saturated after the formation of $L1_2$ phase. The final crystallite size as measured from the XRD peak was found to be 15 nm after 20 h of MA. The arrow in Fig. 1(a) shows the position where the (110) superlattice reflection should appear. Though the lattice parameter matched exactly with that reported for the $L1_2$ phase, no evidence of superlattice reflection was seen.

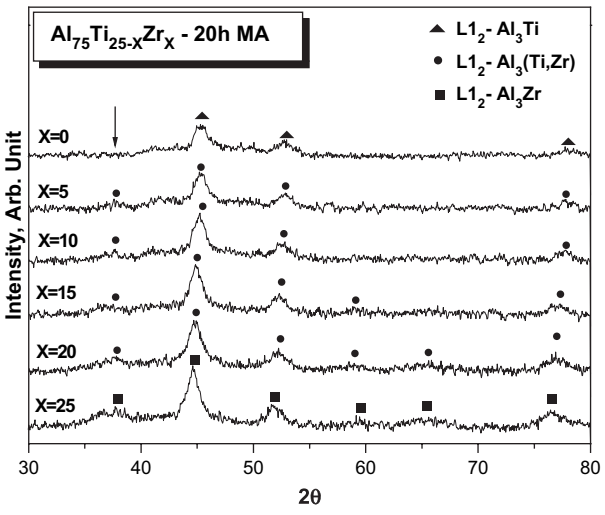

Fig. 3. XRD patterns of $Al_{75}Ti_{25-x}Zr_x$ after 20 h of MA.

$L1_2$ phase forms in binary $Al_{75}Zr_{25}$ composition within 10 h of MA with the strong evidence of superlattice reflections (indicated by arrow in figure) as shown in Fig. 1(b). Even though the formation of $L1_2$ phase has not been observed up to 8 h of MA a slight shift in the Al peaks towards lower diffraction angle was observed, which is attributed to the substitution of Al (0.143 nm) atoms by larger Zr (0.158 nm) atoms leading to the formation of Al(Zr) solid solution. Zr (1 at.%) expands the Al lattice by 0.0012 nm [10]. In the present study the solubility of 2 at.% Zr in Al was found which is quite higher than the equilibrium solubility of 0.0025 at.%. The lattice parameter of $L1_2$-Al_3Zr is exactly same as that reported earlier [9,10,14]. The long range order parameter (S) of $L1_2$-Al_3Zr was calculated to be 0.67 after 10 h of MA and it decreases to 0.61 after 20 h of MA. The crystallite size of $L1_2$ phase is calculated to be 16 nm, after 10 h of MA. The $L1_2$ phase formed after 10 h of MA is stable on further milling up to 20 h and its crystallite size decreased to 15 nm. It has also been observed that $L1_2$-Al_3Zr forms much faster than $L1_2$-Al_3Ti. This is due to the higher diffusivity of Zr than that of Ti in Al lattice [24]. This could also be attributed to the difference in the enthalpy of formation of both the $L1_2$ phases. Calculations based on Miedema's model [25] shows that $L1_2$-Al_3Zr (−61.8 kJ/mol) has more negative enthalpy of formation than that of $L1_2$-Al_3Ti (−34.2 kJ/mol).

The variation of lattice parameter for binary $Al_{75}Ti_{25}$ composition is plotted in Fig. 2(a). It shows a continuous decrease in lattice parameter of Al with increase in the duration of MA up to 15 h, beyond which no significant change has been observed. The lattice parameter after 15 h of MA is 0.401 nm, which is equivalent to that of $L1_2$-Al_3Ti. Lattice parameter of the mechanically alloyed $Al_{75}Zr_{25}$ is shown as a function of duration of MA in Fig. 2(b). It is clearly observed that the lattice parameter increases to a value of 0.409 nm ($L1_2$-Al_3Zr) within 10 h and becomes saturated till 20 h of MA. Saturation of lattice parameter after the $L1_2$ phase formation indicates the stability of the phase on further milling in both the binary $Al_{75}M_{25}$ (M = Ti, Zr) compositions.

From the above results, it can be concluded that synthesis of $L1_2$-Al_3Ti by MA is more difficult in comparison to $L1_2$-Al_3Zr. Hence, it would be interesting to observe the effect

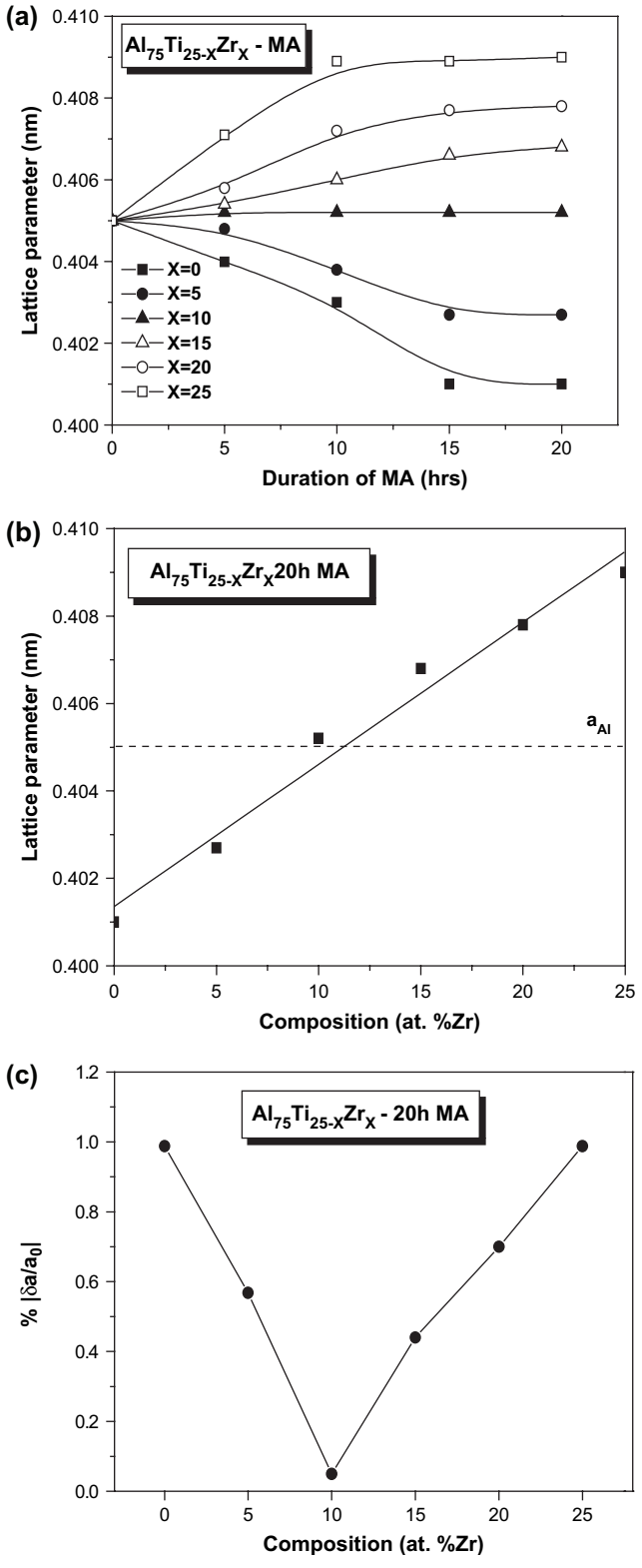

Fig. 4. (a) Variation of lattice parameter of $Al_{75}Ti_{25-x}Zr_x$ after different durations of MA, (b) variation in lattice parameter of $L1_2$-Al_3Ti and (c) percentage change in Al lattice parameter with Zr content in the alloys.

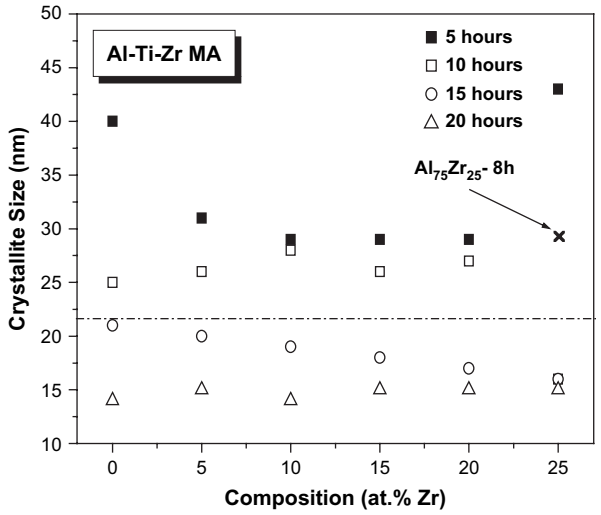

Fig. 5. Variation of crystallite size of $Al_{75}(Ti_{25-x}Zr_x)$ where $x = 5$, 10, 15, 20 and 25 with the duration of MA.

of Zr addition to the $Al_{75}Ti_{25}$ composition on the formation of $L1_2$ phase by MA. Fig. 3 compares the XRD patterns of $Al_{75}(Ti_{25-x}Zr_x)$, $x = 0$, 5, 10, 15, 20 and 25 after 20 h of MA. The formation of $L1_2$ phase was observed in all the compositions studied. The (110) superlattice reflection, marked with the arrow in Fig. 3, is observed in all the compositions except for binary $Al_{75}Ti_{25}$ composition. This suggests that the $L1_2$ phase field extents over the entire composition range studied. The figure also reveals the presence of superlattice peaks of $L1_2$ phase in all the compositions studied, except in binary Al-Ti composition. However, the superlattice reflections become less intense in low Zr containing alloys suggesting that the order parameter of $L1_2$ phase decreases with decrease in Zr content in the alloy. This is due to the large difference in atomic scattering factor between Al and Zr as compared to that in Al and Ti.

It is also clear from Fig. 3 that the fundamental peaks of $L1_2$ phase shift to lower angle with increase in Zr content.

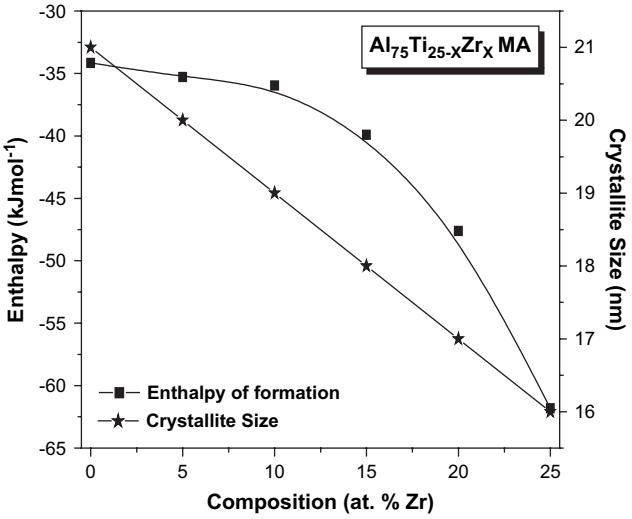

Fig. 7. Correlation between enthalpy of formation and crystallite size of $L1_2$ phase in $Al_{75}Ti_{25-x}Zr_x$.

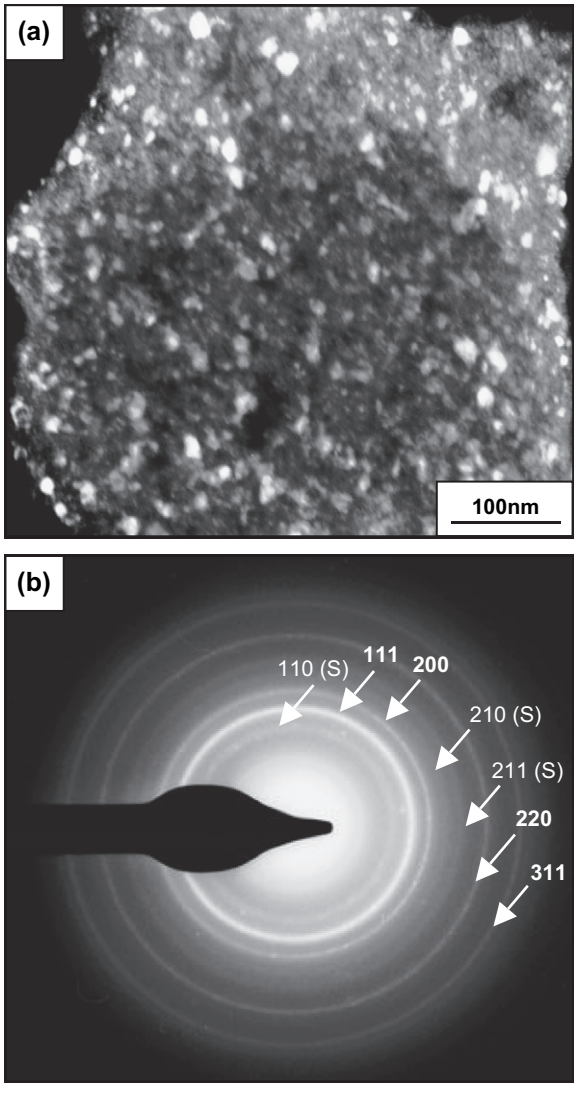

Fig. 6. (a) TEM dark field image and (b) selected area diffraction pattern of nanocrystalline $L1_2$-$Al_{75}Zr_{25}$ after 20 h of MA.

The variation of lattice parameters of all the compositions as a function of the duration of MA is shown in Fig. 4(a). While the Ti rich compositions showed a decrease in the lattice parameter with milling time, the Zr rich compositions showed a reverse trend. The slope of the plot increases with increase in Zr content from negative to positive. With the addition of Zr into $L1_2$-Al_3Ti phase, the lattice parameter increases and reaches that of the $L1_2$-Al_3Zr phase. The plot depicts a gradual transition of $L1_2$-Al_3Ti phase to $L1_2$-Al_3Zr phase with the addition of Zr into binary $Al_{75}Ti_{25}$ composition. Fig. 4(b) shows the variation of lattice parameter of $L1_2$-Al_3(Ti,Zr) after 20 h of MA with the composition in at.% Zr. It clearly shows that the lattice parameter of $L1_2$ phase linearly increases with Zr content. The lattice parameter of $L1_2$-Al_3Ti increases by 0.00032 nm with every 1 at.% Zr addition into the nominal composition of $Al_{75}Ti_{25}$. So it is concluded that the change

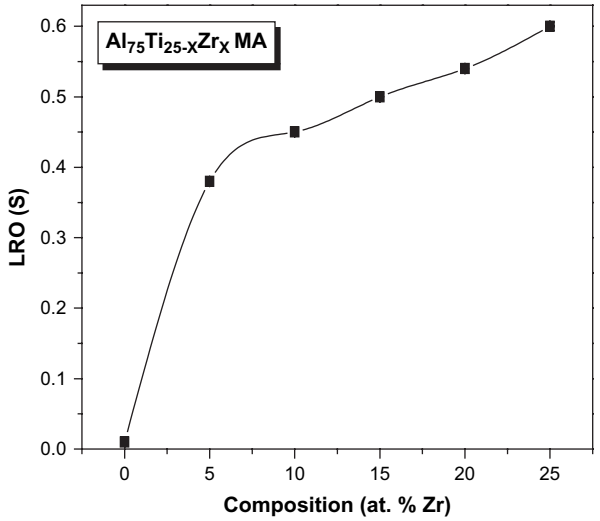

Fig. 8. Variation in S value with composition in at.% Zr for $Al_{75}(Ti_{25-x}Zr_x)$.

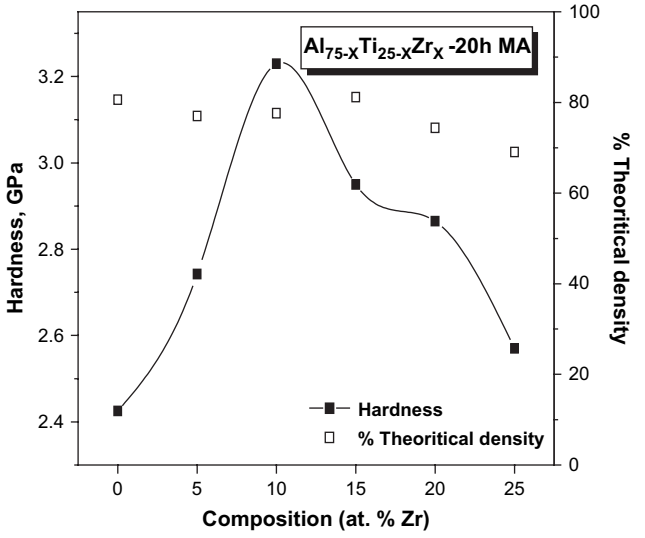

Fig. 9. Hardness and density of the green compacts of nanocrystalline $L1_2$-Al_3(Ti,Zr).

in lattice parameter of $L1_2$-Al_3Ti with Zr addition follows a mathematical relationship of,

$$\left(\frac{a-0.401}{x}\right) = 0.00032\ \text{nm},$$

where a is the new lattice parameter of the $L1_2$ phase when x at.% of Zr enters into $L1_2$-Al_3Ti. The lattice parameter of Al is also shown in Fig. 4(b), which suggests that for compositions less than 10% Zr, the lattice parameter of the $L1_2$ phase is lower than that of Al, while for the higher Zr content, it is higher than that of Al. Interestingly, the lattice parameter of $L1_2$-Al_3Zr phase (0.409 nm) is more as compared to $L1_2$-Al_3Ti phase (0.401 nm) though the atomic radius of both Zr (0.158 nm) and Ti (0.146 nm) is larger than that of Al (0.143 nm). It is known that Ti contracts the Al lattice whereas Zr expands it, which is quite clear from Fig. 4(b). The percentage deviation of the lattice parameter of $L1_2$ phase with respect to Al is plotted as a function of Zr content in the alloys in Fig. 4(c). The difference in the lattice parameter between the $L1_2$ phase and Al is negligible for 10% Zr containing alloy, which is named as the ''neutral composition'' (10 at.% Zr and 15 at.% Ti in Al). Below the ''neutral composition'' Ti remains the dominant solute atom in changing the lattice parameter of Al and above it Zr dominates.

Fig. 5 depicts the variation of crystallite size with milling time as a function of Zr content in $Al_{75}(Ti_{25-x}Zr_x)$ alloys. In the present study, the final crystallite size found was around 15 nm in all the alloys studied irrespective of their composition. As mentioned earlier, $L1_2$ phase forms only after 10 h of MA in the $Al_{75}Zr_{25}$ composition but in rest of the compositions it forms after 15 h of MA. The crystallite size of $L1_2$-Al_3Zr at the time of its formation is 15 nm, while that for $L1_2$-Al_3Ti is 21 nm. The crystallite size of $L1_2$-Al_3Ti was reduced to 14 nm on further milling up to 20 h. However, no significant change in crystallite size was observed in case of $L1_2$-Al_3Zr on further milling. This suggests that $L1_2$-Al_3Ti is brittle in comparison to $L1_2$-Al_3Zr, as brittle materials become finer compared to ductile materials during MA when subjected to same milling conditions. The crystallite size of the intermetallic at the time of its formation decreases with increase in Zr content of the compound. The dark field image and the selected area diffraction (SAD) pattern of the $Al_{75}Zr_{25}$ alloy after 20 h of MA are shown in Fig. 6(a) and (b), respectively. The dark field image shows the presence of nanocrystalline $L1_2$-Al_3Zr spheroids of radius around 15 nm. The crystallite size observed from the TEM photomicrographs matches exactly with the calculated values (15 nm) from the X-ray peak broadening. The SAD pattern confirms the formation of $L1_2$-Al_3Zr after 20 h MA, with the evidence of superlattice rings marked (S) in Fig. 6(b). The solid rings confirm nanocrystalline nature of the $L1_2$-Al_3Zr intermetallic.

Fig. 7 shows the variation of crystallite size of $L1_2$ at the time of its formation and the enthalpy of its formation calculated from Miedema's model [25] with the Zr content. The figure clearly reveals strong correlation between the crystallite size of the ordered intermetallic at the stage of its formation and the enthalpy of its formation. Both crystallite size and enthalpy of formation decrease with increase in Zr content. This suggests that a higher negative enthalpy of formation of the intermetallic leads to finer crystallite size of the compound.

The intensity of (110) superlattice peak of fully ordered $L1_2$-Al_3Zr intermetallic was calculated theoretically to be

Table 1
Comparison of lattice parameter, enthalpy of formation, crystallite size, relative green density, hardness and yield strength of $L1_2$ phase in $Al_{75}Ti_{25-x}Zr_x$ alloys after 20 h of MA

Composition ($Al_{75}Ti_{25-x}Zr_x$)	Lattice parameter of $L1_2$ phase (nm)	ΔH_f (kJ/mol)	CS_f[a] (nm)	Relative green density (%)	Hardness (GPa)	Equivalent YS (=H/2.6) (GPa)
$x=0$	0.4010[b]	−34.16	21	80.6	2.43	0.935
$x=5$	0.4027[c]	−35.28	20	77.0	2.74	1.054
$x=10$	0.4052[c]	−35.96	19	77.6	3.23	1.242
$x=15$	0.4068[c]	−39.92	18	81.2	2.95	1.135
$x=20$	0.4078[c]	−47.61	17	74.4	2.87	1.104
$x=25$	0.4090[d]	−61.81	16	70.1	2.57	0.989

[a] Crystallite size at which the $L1_2$ phase forms.
[b] $L1_2$-Al_3Ti.
[c] $L1_2$-Al_3(Ti,Zr).
[d] $L1_2$-Al_3Zr.

Table 2
Comparison of hardness value, microstructure and processing route of Al alloys

System/composition	Processing route	Phases present	Hardness[a] (GPa)	Reference
$Al_{75}Ti_{25-x}Zr_x$, where $x = 0$, 5, 10, 15, 20 and 25	MA	$L1_2$-Al_3(Ti,Zr)	2.43–3.23	Present work
$Al_{75}(Ti_{1-x}Zr_x)$, where $0 < x < 1$	Arc melting	$DO_{22} + DO_{23}$ Al_3(Ti,Zr)	2.7–3.7	[17]
$Al_{66}Mn_9Ti_{25-x}Zr_x$, where $0 < x < 25$	Conventional casting	$L1_2$-Al_3(Ti,Zr)	1.6–4.0	[18]
Al-Al_3Zr	Inert gas condensation	α-Al + $L1_2$-Al_3Zr	0.8–2.1	[16]
$Al_{89}Ni_{10}Zr_1$	RSP + HT at 423 K	α-Al + Al_3Ni + $L1_2$-Al_3Zr	4.0	[29]
Al-X–Zr (X = Si, Cu, Ni)	RSP + annealing	α-Al + $L1_2$-Al_3Zr	2.5–5	[30]

[a] Hardness values measured in VHN has been converted to GPa.

12% that of the intensity of the (111) fundamental line and is only 2% for $L1_2$-Al_3Ti. The long range order parameter (S) value, calculated after 20 h of MA, as a function of Zr content in the alloy is plotted in Fig. 8. The S value increases from 0 for $Al_{75}Ti_{25}$ to 0.61 for $Al_{75}Zr_{25}$ composition. The plot reveals a sudden rise in the S value when only 5% Zr is added to binary $Al_{75}Ti_{25}$ composition. At higher Zr content, the S value increases moderately with Zr content (Fig. 8). The ordering energy of intermetallics can be estimated from the enthalpy of their formation according to the Bragg–Williams theory $\Delta H_{order} \approx 0.5\Delta H_f$ [26]. As the calculated value of ΔH_f for Al_3Zr is more negative than that of Al_3Ti, the ordering energy of Al_3Zr is more than that of Al_3Ti, which supports the higher S values observed for Al_3Zr in comparison to Al_3Ti. The present results also suggest that completely ordered intermetallic has not been produced in any of the composition in the present study. This can be attributed to the defects induced by high energy ball milling.

The variation of hardness and % theoretical density of green pellets of the $L1_2$ phase as a function of Zr content is shown in Fig. 9. The $L1_2$-Al_3Ti intermetallic shows a hardness of 2.43 GPa with 80% relative density. The hardness increases with the addition Zr into $L1_2$-Al_3Ti and reaches a maximum value of 3.23 GPa for 10% Zr containing intermetallic and then decreases gradually to a value of 2.57 GPa for the $Al_{75}Zr_{25}$ composition ($L1_2$-Al_3Zr). The relative green density was found to be in the range of 70–80% irrespective of the compositions. Table 1 compares relative density, hardness and equivalent yield strength of $L1_2$ phase for different compositions. Yield strength was calculated empirically from the hardness value using the formula $H_v/\sigma_y \approx 2.6$, where σ_y is the Yield strength and H_v is the Vickers hardness. Very high hardness values have been observed in all the alloys studied even at the relative densities of 70–80%. A higher densification is expected to lead to further higher hardness in these intermetallics. The high hardness in the $L1_2$ intermetallic prepared in the present study can be attributed to the nanocrystalline nature of the compound. Guo et al. [27] have reported that an ordered $L1_2$.structure has fewer slip systems than a disordered $L1_2$ structure and if the $L1_2$ structure is disordered it is expected to increase the ductility. So, it can be concluded that the partially disordered nanocrystalline $L1_2$-Al_3(Ti,Zr) prepared in the present might show not only high strength but also good ductility. The work on the ductility of the present intermetallics is under progress [28]. Table 2 compares the hardness values observed in the present study with those reported earlier for similar compounds. It is interesting that even with 70–80% relative densities, the hardness obtained in the present studies is comparable with those obtained for the conventionally cast Al_3(Ti,Zr) [17,18]. Thus, it can concluded that the hardness of 3.23 GPa observed for $L1_2$-Al_3(Ti,Zr) is the highest ever reported hardness value for the compound in the green compact condition. The other reports that are available are for the composites of Al with $L1_2$ phase [16,19,20,29,30] and hence cannot be directly compared with the present results, as single phase intermetallics are reported in the present study. In fact, hardness levels as high as 5 GPa has been observed in the laboratory of the authors in case of nanocomposites of Al and $L1_2$-Al_3(Ti,Zr) [28].

4. Conclusions

1. Nanocrystalline $L1_2$-Al_3(Ti,Zr) has been successfully synthesized directly by MA of nominal composition of $Al_{75}(Ti_{25-x}Zr_x)$ ($x = 0$–25) with a crystallite size of about 15 nm.
2. $L1_2$ phase at $Al_{75}Ti_{15}Zr_{10}$ has the least lattice parameter mismatch with Al.
3. The crystallite size of the $L1_2$ phase at the stage of its formation is proportional to the enthalpy of its formation.
4. Zr increases the long range order parameter of $L1_2$ phase in $Al_{75}(Ti_{25-x}Zr_x)$, leading to a maximum value of 0.61 at 25% Zr.
5. Highest hardness of 3.23 GPa was observed for the $L1_2$ phase at $Al_{75}Ti_{15}Zr_{10}$ in the green compacts with only 77.6% of theoretical density.

Acknowledgements

The present work is sponsored by Department of Science and Technology (grant no. SR/S5/NM-S1/2002) and the Defence Research and Development Organisation (grant no. ERIP/ER-0100169/M/01). One of the authors (S.S. Nayak) acknowledges the financial support of the Council of Scientific and Industrial Research, Govt. of India.

References

[1] Suryanarayana C. Prog Mater Sci 2001;46:1–184.
[2] Murty BS, Ranganathan S. Inter Mater Rev 1998;43(3):101–41.
[3] Koch CC, Whittenberger JW. Intermetallics 1996;4:339–55.

[4] Pabi SK, Murty BS. Mater Sci Eng A 1996;214:146–52.
[5] Dutta MK, Pabi SK, Murty BS. J Appl Phys 2000;87:8393–400.
[6] Yamaguchi M, Ini H. Al_3Ti and its $L1_2$ variations. In: Westbrook JH, Fleischer RL, editors. Intermetallic compounds, vol. 2. New York: Wiley; 1994. p. 147.
[7] Nayak SS, Murty BS. Mater Sci Eng A 2004;367:218–24.
[8] Nayak SS, Murty BS. Trans IIM 2003;56:457–63.
[9] Zhang F, Lu L, Lai MO. J Alloys and Comp 2000;297:211–8.
[10] Jang HS, Kang CW, Kim Y, Hong KT, Kim SJ. Intermetallics 2004;12:477–85.
[11] Virk IS, Varin RA. Scripta Metall Mater 1991;25:85–8.
[12] Desch P, Schwarz RB, Nash P. Scripta Mater 1996;34:37–43.
[13] Suryanarayana C, Wenki Li, Froes FH. Scripta Metall Mater 1994;31:1465–70.
[14] Moon KI, Chang KY, Lee KS. J Alloys Comp 2000;312:273–83.
[15] Lee SH, Moon KI, Lee KS. Intermetallics 2006;14:1–8.
[16] Rittner MN, Eastman JA, Weertman JR. Scipta Metall Mater 1994;31:841–6.
[17] Han SZ, Rho BS, Lee HM, Choi SK. Intermetallics 1996;4:245–9.
[18] Karpets MV, Milman VYu, Barabash OM, Korzhova NP, Senkov ON, Miracle DB. Intermetallics 2003;11:241–9.
[19] Vecchio KS, Williams DB. Acta Metall 1987;35:2959–70.
[20] Guo JQ, Ohtera K, Kita K, Shibata T, Inoue A, Masumoto T. Mater Sci Eng A 1994;181/182:1397–404.
[21] de Keijser TH, Langford JI, Mittemeijer EI, Vogels ABP. J Appl Crystallogr 1982;15:308.
[22] Culity BD. Elements of X-ray diffraction. Addison-Wesley; 1967. p. 372.
[23] Pearson WB. A hand book of lattice spacings and structures of metals and alloys. Oxford: Pergamon; 1974.
[24] Brandes EA, editor. Smithells metals reference book. 6th ed. London: Butterworths; 1983. p. 13–5.
[25] De Boer FR, Room R, Nattens WCM, Miedema AR, Niessen AK. Cohension in metals. In: de Boer FR, Pettifor DG, editors. Cohension and structure, vol. 1. Amsterdam: North Holland; 1989. p. 38.
[26] (Sam) Froes FH, Suryanarayana C, Russell K, Li CG. Mater Sci Eng A 1995;192/193:612–23.
[27] Guo W, Martelli S, Mafini M. Acta Metall Mater 1994;42:411–7.
[28] Nayak SS, Pabi SK, Murty BS. Unpublished work.
[29] Srinivasan D, Chattopadhyay K. Mater Sci Eng A 1998;255:107–16.
[30] Srinivasan D, Chattopadhyay K. Mater Sci Eng A 2004;375–377:1228–34.